Chinese Physics Letters

LETTER

# Charge Density Wave Induced Second-Harmonic Generation in 1T-$TaSe_2$

Cite as: Zhao-Zhe Chen *et al*. 2026 *Chin. Phys. Lett.* **43** 080404

DOI CSTR

## Recommended Articles

**Revealing Light-Induced Charge Density Wave Melting and Carrier Redistribution in 1T-$TiSe_2$**
Wanying Chen, Haoyuan Zhong, Changhua Bao, Fei Wang, Xuanxi Cai, Chenxia Yun, Hao Teng, Zhiyi Wei, and Shuyun Zhou
*Chin. Phys. Lett.* **42**, 017101 (2025)

**Photodoping-Modified Charge Density Wave Phase Transition in $WS_2$/1T-$TaS_2$ Heterostructure**
Rui Wang, Jianwei Ding, Fei Sun, Jimin Zhao, and Xiaohui Qiu
*Chin. Phys. Lett.* **41**, (2024)

**Second Harmonic Generation in Nanowires**
Bi-Jun Zhao, Jian-Lin Zhao, and Xue-Tao Gan
*Chin. Phys. Lett.* **41**, 104201 (2024)

**Second Harmonic-Induced Ultrafast Wrinkle Formation in Two-Dimensional Material**
Xiaodong Wang, Yongzhao Zhang, Shuaishuai Sun, Jun Li, Shaobo Cheng, and Huaixin Yang
*Chin. Phys. Lett.* **42**, 047201 (2025)

**Quantum Metric, Topology and Second Harmonic Generation**
En Wang, Yaxian Wang, and Sheng Meng
*Chin. Phys. Lett.* **42**, 047302 (2025)

**Interplay of Charge Density Wave and Magnetism on the Kagomé Lattice**
Yu-Han Lin, Jin-Wei Dong, Ruiqing Fu, Xianxin Wu, Ziqiang Wang, and Sen Zhou
*Chin. Phys. Lett.* **42**, 080709 (2025)

A series journal of Chinese Physical Society distributed by IOP Publishing

Chinese Physics Letters

*Chin. Phys. Lett.* **43** 080404 (2026)

LETTER

DOI: 10.1088/0256-307X/43/8/080404
CSTR: 32039.14.0256-307X.43.8.080404

# Charge Density Wave Induced Second-Harmonic Generation in 1T-$TaSe_2$

**Zhao-Zhe Chen(陈兆哲)[1,†], Chang-Hua Li(李昌华)[2,3,†], Hai-Xia Zhu(朱海霞)[1], Yan-Peng Qi(齐彦鹏)[2,4,5,*], and Si Xiao(肖思)[1,*]**

[1]Hunan Key Laboratory of Nanophotonics and Devices, School of Physics, Central South University, Changsha 410083, China
[2]State Key Laboratory of Quantum Functional Materials, School of Physical Science and Technology, ShanghaiTech University, Shanghai 201210, China
[3]Zhangjiang Laboratory, Shanghai 201210, China
[4]ShanghaiTech Laboratory for Topological Physics, ShanghaiTech University, Shanghai 201210, China
[5]Shanghai Key Laboratory of High-resolution Electron Microscopy, ShanghaiTech University, Shanghai 201210, China

[†]These authors contributed to this work equally.
[*]Corresponding authors. Email: qiyp@shanghaitech.edu.cn; sixiao@csu.edu.cn

**Charge density wave (CDW) is ordered states characterized by periodic modulation of charge density and accompanying lattice distortions, often leading to superlattice formation and modified electron-phonon coupling. While CDW formation has been extensively studied, its impact on nonlinear optical coefficients remains largely unexplored. Here we report a pronounced second-harmonic generation (SHG) response in centrosymmetric 1T-$TaSe_2$, whose intensity is nearly 20 times that of the 2H phase and exhibits distinct polarization dependence. Temperature-dependent transient absorption spectroscopy reveals a characteristic CDW phonon mode at ~1.88 THz at 463 K, which progressively redshifts and broadens with increasing temperature. Further corroboration was provided by complementary temperature-dependent SHG measurements and corresponding Raman spectroscopic analyses. These findings collectively demonstrate that the inversion symmetry breaking induced by CDW-related lattice distortions is the primary origin of the SHG response observed in 1T-$TaSe_2$. This study reveals that controlling the formation of CDW superlattices through temperature modulation provides an effective avenue for tuning nonlinear optical responses, thereby offering a novel strategy for the rational design of nonlinear optical materials.**

## Introduction

Charge density wave (CDW) is an ordered states involving periodic modulation of the electronic charge density accompanied by lattice distortions. Their formation is commonly associated with superlattice structures and strongly affects electron-phonon coupling and carrier transport [1,2]. CDW also frequently compete or coexist with other correlated quantum phases, including superconductivity [3], magnetism [4], ferroelectricity [5], the Mott states [6,7], and new quantum states such as supercharge-lattice coupling (SCLC) [8]. Consequently, CDW-based superstructures have attracted considerable interest as a route to tailoring material properties. Recent studies have demonstrated promising applications of CDW systems in high on/off ratio electrical switching [9], reconfigurable terahertz optoelectronic logic circuits [10], and gate-controlled resistive switching heterojunction devices [11].

$TaSe_2$ is a prototypical CDW material with localized electronic structure features [12−14], in which the 2H and 1T phases host $3 \times 3$ and $\sqrt{13} \times \sqrt{13}$ CDW superstructures, respectively [12,15]. Despite extensive studies on the CDW modes and their formation mechanisms in $TaSe_2$, the impact of CDW on nonlinear optical responses, especially second-order nonlinear effects, remains poorly understood [16,17]. Since CDW formation is strongly temperature dependent, temperature provides an effective tuning parameter for controlling the formation and evolution of CDW superlattices [15,18]. This process is accompanied by atomic-scale lattice reconstruction, which differs fundamentally from conventional charge-ordering scenarios [19,20]. Importantly, the resulting lattice distortions can modify crystal symmetry and thereby strongly influence the electronic structure, transport, optical and magnetic properties [21,22], as well as the interplay among competing ordered states [23,24].

Here, we systematically study the second-harmonic generation (SHG) response in different phases of $TaSe_2$ and its relation to the CDW state. Remarkably, centrosymmetric 1T-$TaSe_2$ exhibits a strongly enhanced SHG response, with an intensity nearly 20 times larger than that of noncentrosymmetric 2H-$TaSe_2$ and a distinctly different polarization dependence. Temperature-dependent transient absorption measurements further reveal a characteristic CDW phonon mode at ~1.88 THz at 463 K, which undergoes a gradual redshift and broadening upon heating. These results demonstrate that the anomalous SHG response in 1T-$TaSe_2$ arises from inversion symmetry breaking induced by CDW-related lattice distortions. This work establishes temperature-controlled CDW superlattice evolution as an effective route for tuning nonlinear optical responses, providing new opportunities for the design of nonlinear optical functional materials and all-optical logic devices.

## Discussion

High-quality single crystals of 2H-$TaSe_2$ and 1T-$TaSe_2$ were grown and systematically characterized. Detailed crystal growth parameters are provided in the Supplementary Materials (SM). Figure 1(a) shows the schematic crystal structures of the 2H phase (left panel) and the 1T phase (right panel), the corresponding X-ray Diffraction (XRD) patterns are shown in Fig.1(a) (middle panel). Both samples exhibit sharp diffraction peaks, indicative of high crystalline quality. The lattice constants along the *c*-axis are determined to be ~12.23 Å for 2H-$TaSe_2$ and ~6.12 Å for 1T-$TaSe_2$, consistent with literature values [25,26]. The Energy-Dispersive X-ray Spectroscopy (EDS) results shown in Fig. S12 of the SM further confirm a uniform distribution of Ta and Se elements, with elemental ratios close to the nominal stoichiometry. It should be noted that Fig.1(a) presents only the results along the *c*-axis; in fact, 1T-$TaSe_2$ has already undergone a CDW phase transition at room temperature in the in-plane direction, and the corresponding in-plane lattice structure is shown in Fig.S1 of the SM.

Received 26 April 2026; accepted 29 July 2026; published 26 August 2026
© 2026 Chinese Physical Society and IOP Publishing Ltd. All rights, including for text and data mining, AI training, and similar technologies, are reserved.

Check for updates

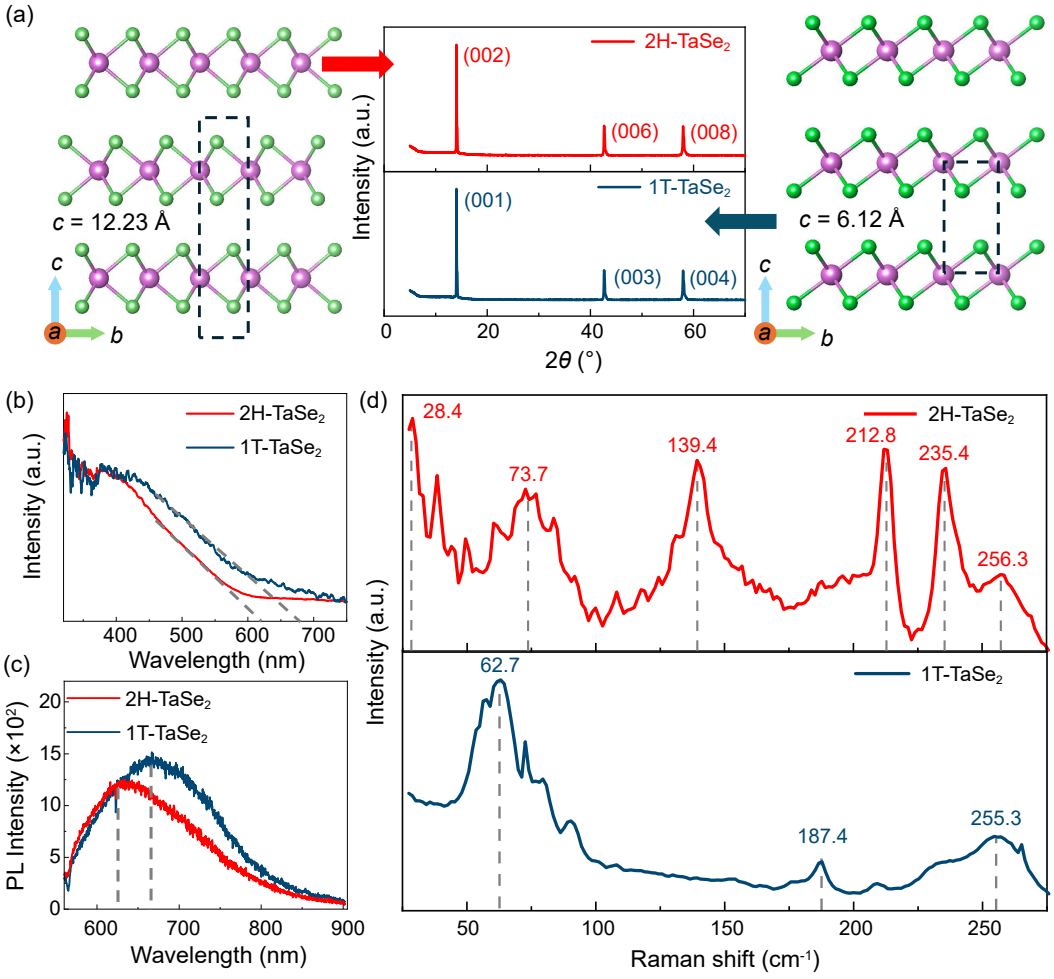


**Fig. 1.** Structural and spectroscopic comparison between 2H-$TaSe_2$ and 1T-$TaSe_2$. (a) Schematic crystal structures and XRD patterns of the 2H and 1T phases. The repeating unit along the *c*-axis is ~12.23 Å for 2H-$TaSe_2$ and ~6.12 Å for 1T-$TaSe_2$, with the latter being approximately half of the former. (b) UV–vis absorption spectra of the 2H and 1T phases. The absorption edges are close, located at ~620 nm for 2H-$TaSe_2$ and ~660 nm for 1T-$TaSe_2$. (c) Photoluminescence spectra of the 2H and 1T phases. The emission peaks are centered at ~625 nm and ~665 nm for 2H-$TaSe_2$ and 1T-$TaSe_2$, respectively. (d) Raman spectra of the 2H and 1T phases. The 2H phase exhibits characteristic peaks at 28.4, 73.7, 139.4, 212.8, 235.4, and 256.3 $cm^{-1}$, whereas the 1T phase shows three major peaks at 62.7, 187.4, and 255.3 $cm^{-1}$.

As shown in Fig. 1(b), the absorption spectra of 2H-$TaSe_2$ and 1T-$TaSe_2$ are highly similar in the visible range, with less than 10% difference in absorption intensity at the same wavelength and nearly identical spectral evolution. Both phases exhibit strong absorption below 400 nm, followed by a gradual decrease with increasing wavelength and a clear turning point near 580 nm, while finite absorption remains above 700 nm. The characteristic absorption features are estimated to be located at ~620 nm and ~660 nm, respectively [27]. Figure 1(c) shows that both phases also exhibit comparable photoluminescence in the 550–900 nm range, with peak centers at ~630 nm and ~670 nm, respectively. These emission features are close to the previously reported characteristic transition energy of ~2.1 eV [7,28], suggesting a high degree of similarity in their linear optical properties.

By contrast, the Raman spectra in Fig. 1(d) reveals substantial differences between the two phases. For 2H-$TaSe_2$, multiple Raman modes are resolved at 28.4, 73.7, 139.4, 212.8, 235.4, and 256.3 $cm^{-1}$, consistent with previous reports [15,29]. In 1T-$TaSe_2$, only three prominent Raman peaks are observed at 62.7, 187.4, and 255.3 $cm^{-1}$ [15,30]. Except for the highest-frequency peak near 255 $cm^{-1}$, the Raman modes differ significantly between the two phases, indicating intrinsic distinctions in lattice dynamics and electron-phonon coupling. These results suggest that, despite their similar structural characterization and linear optical responses, 2H-$TaSe_2$ and 1T-$TaSe_2$ exhibit fundamentally different phonon properties, which may be closely associated with their markedly different second-harmonic generation (SHG) responses. In the following, we discuss the phase-dependent SHG intensity and polarization behavior in greater detail.

Figure 2 summarizes the second-harmonic responses of 2H and 1T-$TaSe_2$ under various excitation wavelengths, powers, and polarization conditions tested at room temperature. We first examine the SHG behavior of 2H-$TaSe_2$. As shown in Fig. 2(a), relatively strong SHG signals are observed under 1000 nm and 1100 nm excitation. The power-dependent measurements in Fig. 2(b) indicate that the SHG intensity decreases rapidly as the excitation power is reduced and approaches the noise floor at low power. Since bulk 2H-$TaSe_2$ is intrinsically centrosymmetric, second-harmonic generation (SHG) is forbidden under the electric-dipole approximation and is allowed only in monolayers, which lack inversion symmetry [31,32]. In this study, however, all the materials investigated are bulk crystals with inversion symmetry; consequently, the observed SHG intensity is relatively weak. As shown in Fig. 2(c), the polarization-resolved SHG of the 2H phase is nearly isotropic in-plane, showing no obvious polarization anisotropy. This value is close to the background signal (~30 counts), indicating that even weaker signals may be obscured by the background, thereby leading to a loss of symmetry information.

By contrast, 1T-$TaSe_2$ shows a markedly different SHG response. Figure 2(d) shows clear SHG signals under excitation wavelengths of 1200, 1100, 1000, and 900 nm, with the strongest response at 900 nm. Notably, under the same experimental conditions, the SHG intensity of the 1T phase is approximately 20 times larger than that of the 2H

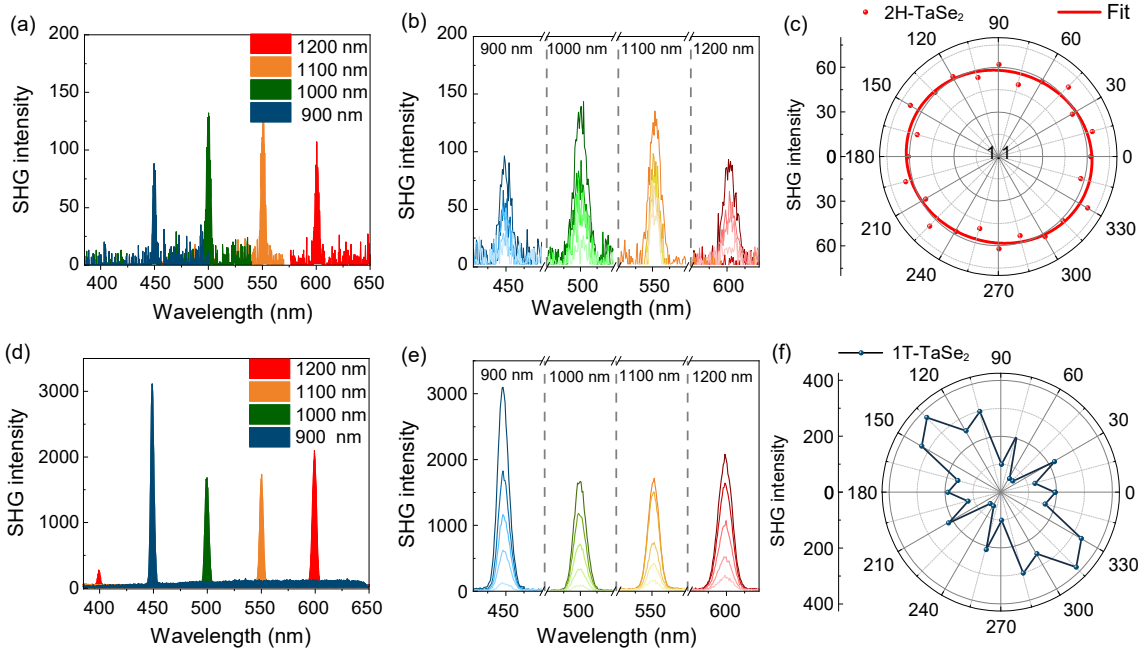


**Fig. 2.** Second-harmonic generation (SHG) of 2H- and 1T-$TaSe_2$ at room temperature. (a) and (d) Excitation-wavelength-dependent SHG spectra of the 2H and 1T phases measured at four fundamental wavelengths from 900 to 1200 nm. The 2H phase shows its strongest SHG response in the 1000–1100 nm range, whereas the 1T phase exhibits the maximum intensity at 900 nm. (b) and (e) Power-dependent SHG intensities of the 2H and 1T phases measured over an input power range of 50–300 μW. (c) and (f) Polarization-resolved SHG patterns of the two phases. The 2H phase exhibits an almost isotropic SHG response, while the 1T phase shows a strongly anisotropic pattern with pronounced peaks near 137° and 317°, indicating symmetry breaking associated with lattice distortion.

phase. As shown in Fig. 2(e), the SHG intensity increases monotonically with excitation power and follows the quadratic dependence expected for a second-order nonlinear optical process [33].

In the ideal structure, 1T-$TaSe_2$ is centrosymmetric, with octahedral coordination and AA stacking, and thus bulk electric-dipole SHG should be forbidden [34]. However, a strong SHG response is clearly observed. As shown in Fig. 2(f), the polarization-resolved SHG intensity exhibits clear anisotropy, with enhanced signals near 137° and 317° [35]. This discrepancy indicates that the actual room-temperature lattice symmetry of 1T-$TaSe_2$ deviates from the ideal centrosymmetric structure, implying local lattice distortions or inversion-symmetry breaking [36]. (The transient and fluorescence results of the polarization measurements are shown in Figs. S9–S11 of the SM.)

Overall, these results reveal an anomalous SHG response in 1T-$TaSe_2$: despite being nominally centrosymmetric, it exhibits a much stronger SHG signal than the intrinsically noncentrosymmetric 2H phase. The nearly 20-fold enhancement, together with the pronounced polarization anisotropy and the failure of the ideal-symmetry model, strongly points to an additional symmetry-breaking mechanism, likely associated with CDW-induced lattice reconstruction. In Section 7 of the SM, we discussed the possibility of symmetry changes in these materials. Although the crystal structures of the two materials appear similar in room-temperature XRD measurements, 1T-$TaSe_2$ has already undergone a CDW phase transition, whereas 2H-$TaSe_2$ remains in its intrinsic state. Therefore, a direct comparison of the SHG responses of these two materials is insufficient to unambiguously demonstrate the influence of the CDW. To clarify the microscopic origin of this behavior, we next turn to temperature-dependent transient absorption measurements.

Figure 3(a) presents the transient absorption dynamics of 2H-$TaSe_2$. Consistent with the photoluminescence results, a pronounced reduction in the transient absorption signal is observed near 630 nm, which is close to the characteristic absorption peak position (~2.0 eV) reported for thick-film samples in the literature [27,37]. Figure 3(b) shows the transient absorption dynamics of 1T-$TaSe_2$. Compared with the 2H phase, the 1T phase exhibits more pronounced metallic characteristics, with relatively strong transient signals observed over a broad wavelength range from 500 to 720 nm. The kinetic traces of the two phases at a probe wavelength of 600 nm are shown in Fig. 3(c). As can be seen, both phases exhibit similar overall relaxation behaviors. Within the first 1 ps after photoexcitation, the transient absorption signal decreases rapidly, which is most likely caused by the prompt filling of conduction-band states by photoexcited high-energy carriers. This is followed by a fast recovery within approximately 2 ps, which may be attributed to a reduction in the hot-carrier population due to defect trapping or rapid intraband relaxation [38]. Subsequently, the system enters a slow relaxation regime lasting for more than 1 ns, which likely corresponds to carrier recombination from the conduction band to the valence band [39,40].

Notably, the overall transient signal of the 1T phase is significantly stronger than that of the 2H phase, with an amplitude approximately twice as large. In addition, the strongest and longest-lived transient response is observed near 2.1 eV, in good agreement with previous theoretical calculations on localized electronic transition channels associated with charge-density-wave formation [28].

These results indicate that CDW order plays an essential role in modulating carrier relaxation in 1T-$TaSe_2$. Together with the weak photoluminescence emission and enhanced Raman response, the transient absorption data support a picture in which strong electron-phonon coupling and CDW-related local lattice distortion give rise to dominant nonradiative relaxation and possible inversion symmetry breaking [41], thereby contributing to the anomalous nonlinear optical response [42].

To clarify the strength and frequency dependence of electron–phonon coupling in 1T-$TaSe_2$, we performed temperature-dependent transient absorption spectroscopy and extracted the periodic oscillatory component of the transient response to probe coherent phonons [43,44]. Figure 3(d) shows the oscillatory signal isolated at 463 K after subtraction of the exponential electronic decay background. Fast Fourier Transform (FFT) analysis of the residual signal yields an amplitude–frequency spectrum with a dominant mode at 1.88 THz. As shown in the insect of Fig.3(d), the background-subtracted oscillatory trace is well defined. Notably, this mode corresponds closely to the 62.7 $cm^{-1}$ phonon observed in Raman measurements, indicating strong consistency between ultrafast and steady-state vibrational probes. For details of the signal processing and temperature-dependent

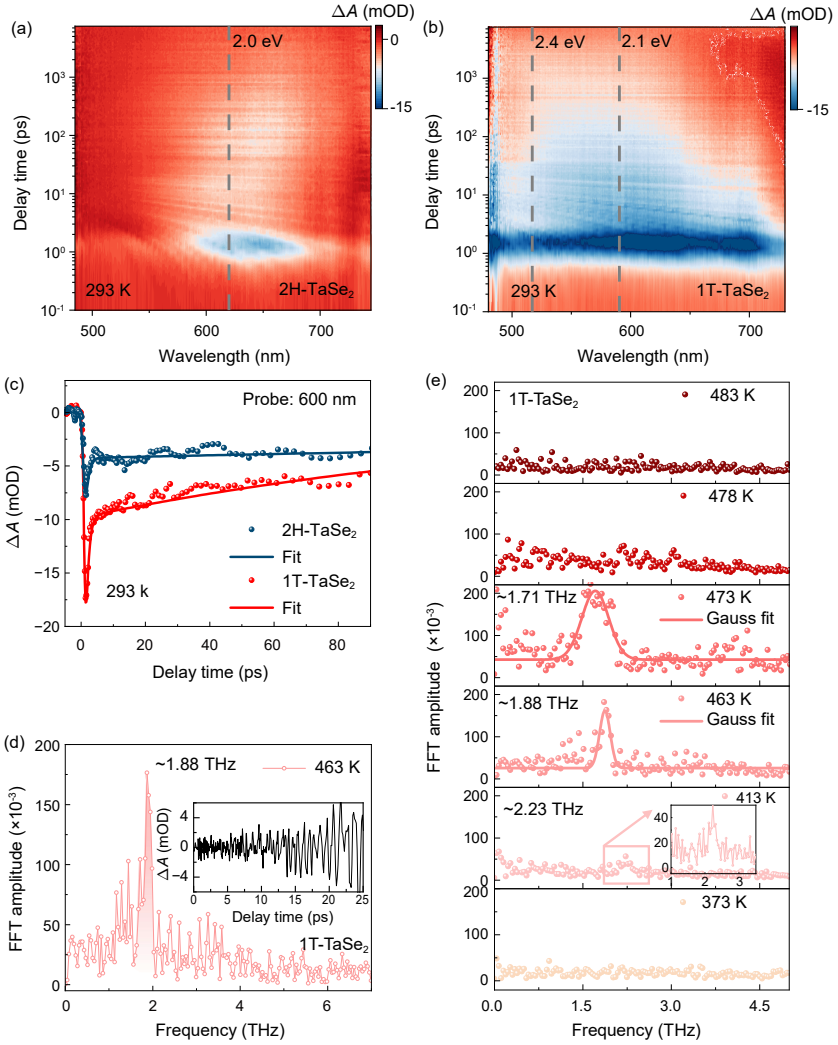


**Fig. 3.** Transient absorption characterization of electron–phonon coupling in 2H- and 1T-$TaSe_2$. (a) and (b) Transient absorption spectra of 2H- and 1T-$TaSe_2$ in the 500–730 nm range. The 2H phase exhibits a distinct feature near 620 nm, corresponding to the fluorescence peak observed in thick films, whereas the 1T phase shows a strong broadband response centered at 2.1 eV, consistent with previously reported transition pathways. (c) Kinetic traces probed at 600 nm for the spectra shown in (a) and (b). Both phases display highly similar dynamics, consisting of a fast relaxation component of ~2 ps followed by a long-lived slower decay. (d) Fast Fourier transform (FFT) amplitude obtained at 463 K under low-power pump–probe conditions, revealing a characteristic coherent mode at ~1.88 THz. The insert shows the oscillatory component extracted after subtraction of the exponential background. (e) Temperature-dependent evolution of the FFT spectra. A characteristic mode at 2.23 THz appears above 413 K, then gradually increases in intensity, broadens, and redshifts with increasing temperature, before disappearing above 473 K.

kinetics, see Figs.S5–S8 of the SM. In addition, temperature-dependent Raman spectroscopy confirms the broadening of the Raman peaks at 473 K, which is associated with the CDW transition.

As shown in Fig. 3(e), a distinct mode first becomes resolvable at 413 K, with a frequency of approximately 2.23 THz, consistent with previously reported CDW-related phonon modes [28,45]. Below this temperature, the oscillatory component is too weak to be clearly identified, likely due to limited signal-to-noise ratio. Upon heating, the oscillation amplitude increases, while the peak frequency continuously redshifts from 2.23 THz to 1.71 THz and the linewidth broadens markedly, consistent with phonon softening in the CDW phase [8]. Because the excitation and probe powers are extremely low (50 nW and ~100 nW, respectively), laser-induced perturbation can be neglected [46]. Gaussian fitting further shows that the mode intensity reaches a maximum near 473 K and then rapidly decreases until disappearing at higher temperatures, in excellent agreement with the reported phase transition temperature of 1T-$TaSe_2$ [7,30,47,48].

These temperature-dependent ultrafast results demonstrate that the evolution of electron–phonon coupling in the 1T phase is closely tied to the formation and melting of the CDW state. The CDW-induced superlattice evolution not only leads to phonon softening and linewidth broadening but also drives continuous reconstruction of the local lattice environment and electron–lattice coupling. More importantly, the associated lattice distortions may further break inversion symmetry in the nominally centrosymmetric 1T structure, thereby activating SHG that would otherwise be forbidden within the electric-dipole approximation [48−51]. In this picture, the anomalously strong SHG response of 1T-$TaSe_2$ arises not from the ideal crystal symmetry itself, but from CDW-driven local structural reconstruction and symmetry lowering.

Furthermore, the results from temperature-dependent SHG and Raman spectroscopy measurements were in agreement with those from transient spectroscopy measurements, further confirming that the CDW phase transition does indeed affect the SHG response [52]. As shown in Fig.4(a), the second-harmonic intensity gradually decreases as the temperature increases from 293 K to 473 K. At 478 K, the signal intensity drops by approximately one order of magnitude, and by 488 K, no discernible harmonic signal is detected. Figure 4(b) presents the extracted peak SHG intensities as a function of temperature. The peak intensity decreases gradually below 473 K, followed by a sharp reduction above this temperature. Notably, the signal recorded at 488 K is comparable to the background level, indicating the absence of any discernible SHG response. Figure 4(c) presents the

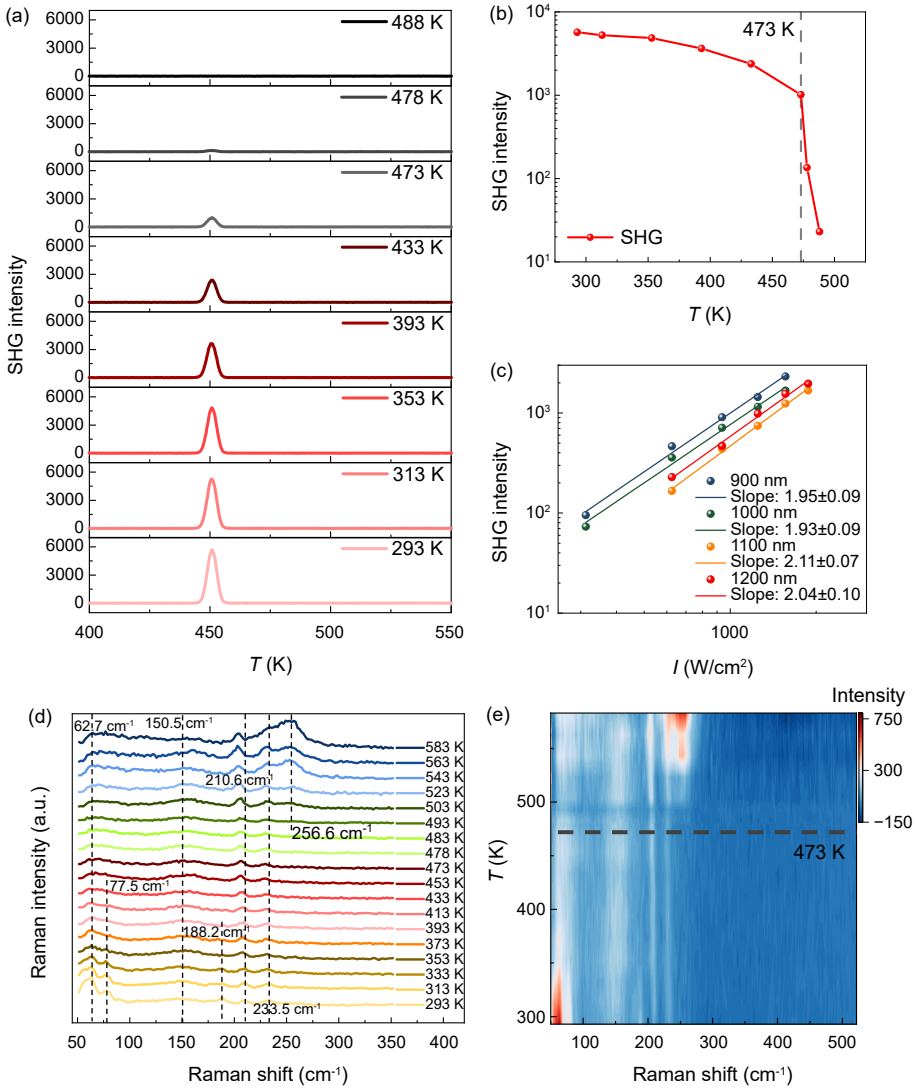


**Fig. 4.** Temperature-dependent second harmonic generation (SHG) and Raman spectroscopy characterization. (a) Under 900 nm pulsed laser excitation, the SHG intensity decreases progressively with increasing temperature. (b) The SHG peak intensity as a function of temperature; above 473 K, a sharp drop in signal intensity is observed, indicating a structural phase transition or the restoration of centrosymmetric in the material. (c) Log-log plot of SHG intensity versus excitation power, where the slope of approximately 2 confirms the second-order nonlinear optical nature of the signal. (d) Raman spectra recorded at various temperatures, showing clear redshifts and broadening of characteristic phonon modes with rising temperature. (e) A false-color map illustrating the evolution of Raman peak positions as a function of temperature, highlighting phonon softening behavior and critical fluctuations near the phase transition.

excitation-power-dependent SHG intensities acquired at excitation wavelengths of 900, 1000, 1100, and 1200 nm, using a beam spot size of approximately 4 μm. The data are displayed on a log–log scale and subjected to linear fitting. The fitted slopes are 1.95, 1.93, 2.11, and 2.04, respectively, all close to the ideal value of 2, thereby confirming the quadratic dependence on excitation power expected for a bona fide SHG response. This behavior verifies that the measured signals arise from second-harmonic generation rather than from other nonlinear optical processes.

Figure 4(d) presents the temperature-dependent Raman spectra of 1T-$TaSe_2$. At room temperature, multiple well-defined Raman peaks are observed at 62.7, 77.5, 150.5, 188.2, 210.6, and 233.5 $cm^{-1}$. As the temperature increases, the two low-frequency modes at 62.7 and 77.5 $cm^{-1}$ gradually merge into a broad spectral feature near 473 K. Meanwhile, the mode located at approximately 188.2 $cm^{-1}$ continuously decreases in intensity, whereas the peaks at 210.6 and 233.5 $cm^{-1}$ undergo pronounced red shifts. In addition, a new Raman feature appears near 256.6 $cm^{-1}$ above 483 K. These observations agree well with previous literature [34], indicating that the Raman response of 1T-$TaSe_2$ is substantially modified by temperature-induced changes associated with CDW behavior. Figure 4(e) summarizes the temperature-dependent evolution of the Raman peak positions. The Raman modes are relatively sharp at room temperature but progressively coalesce into a broad spectral feature upon heating. Moreover, a new high-temperature Raman peak appears at 256.6 $cm^{-1}$.

In contrast, the CDW transition temperature of 2H-$TaSe_2$ is only about 123 K, placing its room-temperature state far from the critical regime [19,29]. As a result, CDW-related fluctuations and superlattice reconstruction are much weaker in the 2H phase than in the 1T phase under the present conditions. This difference naturally explains why 1T-$TaSe_2$ exhibits much stronger CDW-enhanced electron–phonon coupling, local symmetry breaking, and ultimately a far more pronounced nonlinear optical response. These findings provide direct ultrafast evidence for the origin of the anomalous SHG response in 1T-$TaSe_2$ and highlight CDW superlattice evolution as an effective route for tuning second-order nonlinear optical properties.

## Conclusion

In summary, we have systematically investigated the SHG response in different crystal phases of $TaSe_2$ and elucidated its correlation with the CDW state. Notably, a pronounced SHG signal was

observed in the nominally centrosymmetric 1T-$TaSe_2$ phase, with an intensity approximately 20 times stronger than that of 2H-$TaSe_2$ and displaying distinctly different polarization dependence. Temperature-dependent transient absorption spectroscopy further reveals a characteristic CDW phonon mode at ~1.88 THz, which exhibits continuous redshift and spectral broadening upon heating, consistent with the evolution of the CDW state. Temperature-dependent SHG measurements combined with Raman spectroscopy further confirm that the enhanced SHG in 1T-$TaSe_2$ originates from the breaking of inversion symmetry induced by CDW-related lattice distortions. Our work identifies CDW superlattice formation as an effective route to engineer second-order nonlinear optical responses and provides a basis for developing tunable nonlinear optical and all-optical logic devices based on correlated materials.

## Acknowledgments

This work was supported by the National Natural Science Foundation of China (Grant No. 12574369), the Hunan Provincial Top-level Fund (Grant No. 2025JJ50377), and the Key Project of Hunan Provincial Department of Education (Grant No. 24A0019).

## References

[1] Kountz E D, Zhang J, Straquadine J A W, Singh A G, Bachmann M D, Fisher I R, Kivelson S A, and Kapitulnik A 2021 *Phys. Rev. B* **104** L241109
[2] Nie L, Sun K, Ma W, Song D, Zheng L, Liang Z, Wu P, Yu F, Li J, Shan M, Zhao D, Li S, Kang B, Wu Z, Zhou Y, Liu K, Xiang Z, Ying J, Wang Z, Wu T, and Chen X 2022 *Nature* **604** 59
[3] Lin T, Wang X, Chen X, Liu X, Luo X, Li X, Jing X, Dong Q, Liu B, Liu H, Li Q, Zhu X, and Liu B 2021 *Inorg. Chem.* **60** 11385
[4] Lin Y H, Dong J W, Fu R, Wu X, Wang Z, and Zhou S 2025 *Chin. Phys. Lett.* **42** 080709
[5] Huang Y T, Li Z Z, Chen N K, Wang Y, Sun H B, Zhang S, and Li X B 2024 *Nat. Commun.* **15** 9983
[6] Avigo I, Queisser F, Zhou P, Ligges M, Rossnagel K, Schützhold R, and Bovensiepen U 2020 *Phys. Rev. Res.* **2** 022046
[7] Chen Y, Ruan W, Wu M, Tang S, Ryu H, Tsai H Z, Lee R L, Kahn S, Liou F, Jia C, Albertini O R, Xiong H, Jia T, Liu Z, Sobota J A, Liu A Y, Moore J E, Shen Z X, Louie S G, Mo S K, and Crommie M F 2020 *Nat. Phys.* **16** 218
[8] Hasaien J, Wu Y, Shi M Z, Zhai Y N, Wu Q, Liu Z, Zhou Y, Chen X H, and Zhao J M 2025 *Proc. Natl. Acad. Sci. U.S.A.* **122** e2406464122
[9] Hart J L, Siddique S, Schnitzer N, Funni S D, Kourkoutis L F, and Cha J J 2023 *Nat. Commu.* **14** 8202
[10] Sun X, Xiao K, Wei Y, Mo W, Zhang L, Tian S, Pan X, Yang Y, Lan S, Zhang Y, Hu Z, Zhang K, Han L, Wang F, Chen X, Wang L, and Hu W 2025 *Nat. Commun.* **16** 4736
[11] Mahajan M, Murali K, Kawatra N, and Majumdar K 2019 *Phys. Rev. Appl.* **11** 024031
[12] Huang B, Wang L, Ma N, Li K, Song J, Chen G, and Li A 2021 *Phys. Rev. B* **104** 115136
[13] Wang H, Chen Y, Zhu C, Wang X, Zhang H, Tsang S H, Li H, Lin J, Yu T, Liu Z, and Teo E H T 2020 *Adv. Funct. Mater.* **30** 2001903
[14] Ryu H, Chen Y, Kim H, Tsai H Z, Tang S, Jiang J, Liou F, Kahn S, Jia C, Omrani A A, Shim J H, Hussain Z, Shen Z X, Kim K, Min B I, Hwang C, Crommie M F, and Mo S K 2018 *Nano Lett.* **18** 689
[15] Tsang J C, Smith J E, Shafer M W, and Meyer S F 1977 *Phys. Rev. B* **16** 4239
[16] Chen W Y, Zhong H Y, Bao C H, Wang F, Cai X Y, Yun C X, Teng H, Wei Z Y, and Zhou S Y 2025 *Chin. Phys. Lett.* **42** 017101
[17] Tian Z Y, Li S Y, Zhou H T, Jiang Y H, and Mao J H 2025 *Chin. Phys. B* **34** 027301
[18] Ruggeri M, Wolverson D, Romano V, Cerullo G, Sayers C J, and D'Angelo G 2024 *Phys. Rev. B* **110** 165153
[19] Tymoshenko Y, Haghighirad A A, Heid R, Lacmann T, Ivashko A, Merritt A, Shen X, Merz M, Garbarino G, Paolasini L, Bosak A, Diekmann F K, Rossnagel K, Rosenkranz S, Said A H, and Weber F 2025 *Commun. Phys. Physics* **8** 352
[20] Hovden R, Tsen A W, Liu P, Savitzky B H, El Baggari I, Liu Y, Lu W, Sun Y, Kim P, Pasupathy A N, and Kourkoutis L F 2016 *Proc. Natl. Acad. Sci. U. S. A.* **113** 11420
[21] Cao Z Y, Chen H, Qian G J, Shi Y H, Qi Q, Han X H, Yang H T, and Gao H J 2025 *Chin. Phys. Lett.* **42** 100702
[22] Xu Z, Le T, and Lin X 2025 *Chin. Phys. Lett.* **42** 037304
[23] Wang R, Ding J W, Sun F, Zhao J M, and Qiu X H 2024 *Chin. Phys. Lett.* **41** 057801
[24] Cao W Z, Su Y L, Wang Q, Pei C Y, Gao L L, Zhao Y, Li C H, Yu N, Wang J H, Liu Z K, Chen Y L, Li G, Li J, and Qi Y P 2022 *Chin. Phys. Lett.* **39** 047501
[25] Bierman B C, Nolan G, Ma H, Wang Y, Huang P, and Rhodes D A 2025 *J. Am. Chem. Soc.* **147** 39093
[26] Wiegers G A, de Boer J L, Meersma A, and van Smaalen A 2001 *Z. Kristallogr* **216** 45
[27] Mahajan M, Kallatt S, Dandu M, Sharma N, Gupta S, and Majumdar K 2019 *Commun. Phys.* **2** 88
[28] Sayers C J, Dal Conte S, Wolverson D, Gadermaier C, Cerullo G, Carpene E, and Da Como E 2022 *Adv. Opt. Mater.* **10** 2200362
[29] Hajiyev P, Cong C, Qiu C, and Yu T 2013 *Sci. Rep.* **3** 2593
[30] Yan J A, Cruz M A D, Cook B, and Varga K 2015 *Sci. Rep.* **5** 16646
[31] Chowdhury S, Simpson J R, Einstein T L, and Hight Walker A R 2019 *Phys. Rev. Mater.* **3** 084004
[32] Luo R H, Liu S Y, Dong X, Tian J G, and Liu Z B 2026 *Chin. Phys. B* **35** 034201
[33] Xu Y Z, Li Z L, Zhang A N, Liu K, Zhang J J, Wang X J, Peng Q J, and Xu Z Y 2024 *Chin. Phys. B* **33** 014206
[34] Samnakay R, Wickramaratne D, Pope T R, Lake R K, Salguero T T, and Balandin A A 2015 *Nano Lett.* **15** 2965
[35] Kumar N, Najmaei S, Cui Q, Ceballos F, Ajayan P M, Lou J, and Zhao H 2013 *Phys. Rev. B* **87** 161403(R)
[36] Zhao H, An Q, Ye X, Yu B H, Zhang Q H, Sun F, Zhang Q Y, Yang F, Guo J, and Zhao J 2021 *Nano Energy* **82** 105752
[37] Huang P P, Zhang Y L, Hu K, Qi J B, Zhang D N, and Cheng L 2024 *Chin. Phys. B* **33** 017201
[38] Zhang Y, Shi X, You W, Tao Z, Zhong Y, Cheenicode Kabeer F, Maldonado P, Oppeneer P M, Bauer M, Rossnagel K, Kapteyn H, and Murnane M 2020 *Proc. Natl. Acad. Sci. U.S.A.* **117** 8788
[39] Jiang L T, Jiang C Y, Tian Y C, Zhao H, Zhang J, Tian Z Y, Fu S H, Liang E J, Wang X C, Jin C Q, and Zhao J M 2024 *Chin. Phys. Lett.* **41** 047802
[40] Lu S Y, Zhang Y Q B, Ma X, Li J, Deng Y K, and Liu Y Q 2025 *Chin. Phys. Lett.* **42** 017303
[41] Yang R, Zhu Y Y, Steigleder M, Liu Y C, Liu C C, Qiu X G, Zhang T, and Dressel M 2025 *Phys. Rev. Lett.* **134** 196905
[42] Urban J M, Spencer M S, Frenzel M, Trippé-Allard G, Cherasse M, Berrezueta-Palacios C, Joshi P P, Fellows A P, Minakova O, Barros E B, Perfetti L, Reich S, Wolf M, Deleporte E, and Maehrlein S F 2026 *Adv. Mater.* **38** e02204
[43] Chen Z Z, Liu S, Li J, Zhu H X, Wang Y W, Xiao S, Zhong M Z, and He J 2026 *Newton* **2** 100474
[44] Heinrich T, Chang H T, Zayko S, Rossnagel K, Sivis M, and Ropers C 2023 *Phys. Rev. X* **13** 021033
[45] Shi X, You W J, Zhang Y C, Tao Z S, Oppeneer P M, Wu X X, Thomale R, Rossnagel K, Bauer M, Kapteyn H, and Murnane M 2019 *Sci. Adv.* **5** eaav4449
[46] Sayers C J, Hedayat H, Ceraso A, Museur F, Cattelan M, Hart L S, Farrar L S, Dal Conte S, Cerullo G, Dallera C, Da Como E, and Carpene E 2020 *Phys. Rev. B* **102** 161105
[47] Wilson J A, Di Salvo F J, and Mahajan S 1974 *Phys. Rev. Lett.* **32** 882
[48] Ji S, Grånäs O, Rossnagel K, and Weissenrieder J 2020 *Phys. Rev. B* **101** 161105
[49] Fichera B T, Kogar A, Ye L, Gökce B, Zong A, Checkelsky J G, and Gedik N 2020 *Phys. Rev. B* **101** 241106
[50] Pike N A and Pachter R 2021 *J. Phys. Chem. C* **125** 11075
[51] Zhu H X, Xiao S, Wang Y W, Zhong M Z, and He J 2026 *Appl. Phys. Lett.* **7** 071103
[52] Sun F, Wu Q, Wu Y L, Zhao H, Yi C J, Tian Y C, Liu H W, Shi Y G, Ding H, Dai X, Richard P, and Zhao J 2017 *Phys. Rev. B* **95** 235108